# An Analysis of the Low Temperature, Low and High Strain-Rate Deformation of Ti-6Al-4V

P.S. FOLLANSBEE and G.T. GRAY, III

The deformation behavior of Ti-6Al-4V at temperatures between 76 and 495 K, strain rates between 0.001 and 3000 $s^{-1}$, and compressive strains to 0.3 has been investigated. Measurements of yield stress as a function of test temperature, strain rate, and prestrain history are analyzed according to the model proposed by Kocks and Mecking. The mechanical threshold stress (flow stress at 0 K) is used as an internal state variable, and the contributions to the mechanical threshold stress from the various strengthening mechanisms present in this alloy are analyzed. Transmission electron microscopy (TEM) is used to correlate deformation substructure evolution with the constitutive behavior. The deformation substructure of Ti-6-4 is observed to consist of planar slip in the $\alpha$ grains at quasistatic strain rates. At high strain rates, deformation twinning is observed in addition to planar slip. Increasing the temperature to 495 K is seen to alter the deformation mode to more random slip; the effect of this on the proposed deformation model is discussed.

## I. INTRODUCTION

TITANIUM alloys, particularly $\alpha + \beta$ alloys such as Ti-6Al-4V (hereafter, Ti-6-4), have seen extensive use in the metals industry due to their high specific strengths and corrosion resistance. The microstructures of $\alpha + \beta$ alloys are known to depend strongly on both processing history and on heat treatment. This enables a variety of transformation products to be selected, the morphology, volume fraction, and distribution of which can be varied by the appropriate combination of heat treatment and processing. The ability to tailor the microstructure of titanium alloys allows a high degree of control over the mechanical properties of these materials, and there have been several comprehensive reviews of structure/property relations in titanium-based alloys.[1,2]

While extensive experimental data are available for face-centered cubic and body-centered cubic metals, the strain-rate response of hexagonal-close-packed metals, particularly alloys, remains poorly investigated. The purpose of this paper is to report details of an investigation of the strain-rate sensitivity, work hardening, and substructure development of Ti-6-4. Results will concentrate on studies of Ti-6-4 processed to yield an equiaxed alpha microstructure. Results of Ti-6-4 processed to give different microstructural conditions will be discussed also. The major emphasis will be the analysis of quasistatic strain rates, but measurements at strain rates to 3000 $s^{-1}$ are also described. The mechanical properties are analyzed in accordance with the procedure proposed by Kocks[3] and Mecking and Kocks.[4] Emphasis is placed upon examining how this simple modeling approach can be applied to a more complex alloy, like the two-phase alloy Ti-6-4, where strengthening is the result of a multiplicity of strengthening mechanisms. To assist the application of the Kocks/Mecking model to the analysis of deformation in Ti-6-4, analysis of measurements by Paton *et al.* in Ti-Al binary alloys[5] is described also.

P.S. FOLLANSBEE and G.T. GRAY, III are Staff Members of Los Alamos National Laboratory, Los Alamos, NM 87545.

Manuscript submitted December 4, 1987.

The approach of this paper will be first to review in Section II the Kocks/Mecking model. A comparison is made between the model and that previously applied by Conrad and coworkers[6–10] to the deformation of pure titanium and titanium alloys over a wide temperature regime. Differences between the two approaches are examined in Section II–C. The experimental procedure for the measurements reported here is outlined in Section III and results are presented in Section IV. The measurements indicate a lack of the strong increased strain-rate sensitivity often observed at strain rates exceeding $10^3$ $s^{-1}$. The temperature and strain-rate dependence of the yield and flow stress is analyzed according to the Kocks/Mecking model in Section V, and constitutive relations based on this model are derived, tested, and discussed. The results are summarized in Section VI.

## II. THE KOCKS/MECKING MODEL

### A. *Thermal Activation at Constant Structure*

We consider deformation at temperatures below the diffusion controlled regime and at strain rates below the dislocation drag or velocity controlled regime and assume that deformation is controlled by the thermally activated interactions of dislocations with obstacles. Typically, this process is described with an equation of the form:

$$\left(\frac{\hat{\tau}}{\mu}\right)^n = \left(\frac{\tau_a}{\mu}\right)^n + \sum_{i=1}^{r}\left[\left(\frac{\hat{\tau}_i}{\mu}\right)\right]^n$$

or

$$\left(\frac{\tau}{\mu}\right)^n = \left(\frac{\tau_a}{\mu}\right)^n + \sum_{i=1}^{r}\left[s_i\,(\dot{\gamma}, T)\left(\frac{\hat{\tau}_i}{\mu}\right)\right]^n \qquad [1]$$

where $\mu$ is the shear modulus; $\tau$ is the yield stress; $\tau_a$ is an athermal stress; $\hat{\tau}_i$ is the mechanical threshold stress that characterizes the stress at 0 K that is required to force a dislocation past the obstacles identified with the subscript $i$; $\hat{\tau}$ is the total mechanical threshold stress; and $s_i$ is the ratio between the yield stress at any strain rate

($\dot{\gamma}$) and temperature ($T$) and the yield stress at 0 K. Equation [1] is summed over all ($r$) types of obstacles. For Ti-6-4, potential obstacles include forest dislocations, interstitial and solute atoms, and ordered $Ti_3Al$ precipitates. The constant $n$ describes how the summation is performed, *i.e.*, linear ($n = 1$), sum of squares ($n = 2$), *etc.* We emphasize that Eq. [1] is an approximation used to model the complicated interactions that occur when multiple obstacles are present. Kocks, Argon, and Ashby[11] and Kocks[12] have discussed the application of Eq. [1] to specific summed deformation mechanisms and have concluded that linear summation applies only when many short-range obstacles (*e.g.*, a Peierls barrier) are summed with a few long-range obstacles (*e.g.*, dislocations or dispersoids). The thought is that the sum of squares law should better describe the case when the obstacles are similar in character. However, there exist no precise guidelines for choosing the exponent in Eq. [1]; thus, in this paper we will evaluate the measurements according to Eq. [1], assuming linear summation as a first approximation. For the ratio $s_i$, we follow Kocks *et al.*[11] and write the phenomenological expression:

$$\dot{\gamma} = \dot{\gamma}_{o_i} \exp\left(\frac{-\Delta G_i}{kT}\right)$$

$$= \dot{\gamma}_{o_i} \exp\left\{\frac{-g_{o_i}\mu \mathbf{b}^3}{kT}\left[1 - \left(\frac{\tau_i/\mu}{\hat{\tau}_i/\mu}\right)^{p_i}\right]^{q_i}\right\} \qquad [2]$$

where $\Delta G_i$ is the activation free enthalpy, or the Gibbs free energy of activation (for obstacle $i$); $g_{o_i}$ is the normalized total activation free enthalpy; k is Boltzmann's constant; $\mathbf{b}$ is the Burgers vector; $\tau_i$ is the applied stress (minus any athermal component); and $p_i$, $q_i$, and $\dot{\gamma}_{o_i}$ are assumed to be constants. Normalization of the stresses by the temperature dependent shear modulus originates from the derivations of the mechanical threshold stress for dislocation/dislocation interactions,

$$\hat{\tau}_D = \alpha_D \mu \mathbf{b} \sqrt{\rho} \qquad [3]$$

where $\rho$ is the total dislocation density and $\alpha_D$ is a geometric factor, and for dislocation/solute, $\hat{\tau}_S$, or dislocation/interstitial interactions, $\hat{\tau}_I$,

$$\hat{\tau}_C = \alpha_C \mu \sqrt{C} \qquad [4]$$

where $C$ is the concentration and $\alpha_D$ is another geometric factor. The shear modulus also is factored out of the activation free enthalpy to reflect the same temperature dependency.[11]

First, we emphasize that Eq. [2] is assumed to describe the main features of dislocation/obstacle interactions. Whether $\dot{\gamma}_{o_i}$ indeed is independent of stress and temperature and whether the correct temperature dependencies have been introduced are important issues that are difficult to resolve. Second, the application of Eq. [2] must meld with an understanding of the operative deformation mechanisms. Changes in the deformation mechanisms will be reflected by changes in the fit to Eq. [2], and extrapolation beyond the range of validity must be avoided. This is important particularly in titanium alloys, which deform by such a complex combination of mechanisms.

### B. *Structure Evolution*

We assume that microstructural evolution occurs only by the accumulation of dislocations during strain hardening and model the hardening rate, or evolution of the mechanical threshold stress for dislocation/dislocation interactions, through

$$\frac{d\hat{\tau}_D}{d\gamma} = \Theta_o\left[1 - F\left(\frac{\hat{\tau}_D}{\hat{\tau}_{Ds}(\dot{\gamma}, T)}\right)\right] \qquad [5]$$

where $\Theta_o$ is the Stage II or athermal hardening rate and $\hat{\tau}_{Ds}$ is the mechanical threshold stress at saturation, *i.e.*, when strain hardening vanishes. When $F = 1$, Eq. [5] represents Voce law behavior.[3] One advantage of Eq. [5] is that strain hardening is described differentially which implies that strain is not assumed to be a state variable, as it is in typical power-law formulations, for instance. The temperature and strain-rate dependence of strain hardening is contained within the saturation stress term. For fcc metals, a model for stress assisted and thermally activated cross slip has been applied to describe $\hat{\tau}_{Ds}(\dot{\gamma}, T)$[13,3,14] according to

$$\ln\left(\frac{\dot{\gamma}}{\dot{\gamma}_{Ds}}\right) = \frac{-A}{kT} \ln\left(\frac{\hat{\tau}_{Ds}}{\hat{\tau}_{Ds_o}}\right) \qquad [6]$$

where $\dot{\gamma}_{Ds}$ and $A$ are constants and $\hat{\tau}_{Ds_o}$ is the saturation value of the mechanical threshold stress for deformation at 0 K. The potential application of Eq. [6] to describe dynamic recovery in Ti-6-4 will be discussed in Section V.

Equations [1] through [6] have been formulated in terms of the resolved shear stress $\tau$ and shear strain $\gamma$. In Section V, we fit compression test results to these expressions and, to avoid the use of a Taylor factor, we replace these equations with their counterparts formulated in terms of axial stress $\sigma$ and axial strain $\varepsilon$.

### C. *Comparison with Previous Models for the Deformation of Titanium*

The deformation kinetics and work hardening behavior of pure titanium and titanium alloys have been analyzed in detail by Conrad and coworkers.[6–10] For pure titanium, their analysis of the thermal activation behavior is similar to that described by Eqs. [1] and [2]. One difference is that, in the previous work, dislocation/dislocation interactions were assumed to contribute only to the athermal stress component. Thus, the athermal stress increased with strain (and these investigators used a power law dependence).[15,8] The strain-rate sensitivity of the flow stress, measured using strain-rate jump tests, was found to increase with strain,[15] to decrease with strain,[10] or to remain relatively constant with strain.[16] A minor difference also is noted in the form of Eq. [2] used in this previous work, where agreement was obtained when the stresses and activation enthalpy were not normalized by the temperature dependence of the shear modulus.[7] Based on their results, Conrad *et al.* concluded that deformation in pure titanium is controlled by the interactions of dislocations with interstitial atoms,[8] and they introduced the concept of the equivalent oxygen content

($O_{eq}$ = O + 2N + 0.75C) and found general agreement with Eq. [4]. Because dislocation/dislocation interactions are relatively strain-rate insensitive (although still strain-rate dependent) and because the temperature dependent shear modulus does not introduce a large effect in Eq. [2], the analysis of Conrad *et al.* of deformation in pure titanium is consistent with the approach outlined in Section II–A.

The deformation of Ti-6-4 was studied by de Meester, Doner, and Conrad[16] using the same methodology applied to pure titanium. An important distinction in this work is that the authors concluded that the solution hardening contribution also belonged in the athermal stress term. This conclusion was based on the apparent plateau in the variation of yield stress with temperature at temperatures exceeding 538 K. After subtracting this large athermal stress (≈500 MPa) from the total stress, analysis of the remaining stress yielded similar conclusions to those reached for pure titanium regarding the importance of dislocation/interstitial interactions as the rate controlling deformation mechanism. These conclusions follow from the measured athermal stress. However, this usage of the plateau to indicate the athermal stress component in titanium has been criticized by several investigators.[17,18] A plateau in the yield stress *vs* temperature plot may indicate the contribution of dynamic strain aging[19] or may indicate a subtle change in deformation mechanism that could not be modeled using a single form of Eq. [2]. For instance, a change from planar to wavy slip, leading to a plateau in the yield stress *vs* temperature curve, has been documented in Ti-Al binary alloys as the temperature is increased, where the transition temperature depends on Al contents.[5] This same study indicated that in Ti-10.2 pct Al a transition from $\bar{c} + \bar{a}$ slip to predominately $\bar{c}$ slip occurs at a temperature of 575 K.[5] Thus, it is possible that the temperature dependence of the yield stress may decrease due to several competing deformation mechanisms and yet give the appearance of the approach to an athermal stress.

Therefore, in the analysis of Ti-6-4 deformation that follows, we will follow Eq. [1] and assume that dislocation/dislocation interactions and dislocation/solute interactions are strain-rate dependent. The remaining athermal stress $\tau_a$ is a small term representing only true long-range interactions (with grain boundaries, for instance). Several features of the previous work[8] will be retained. For example, this previous work indicated that the constants $p$ and $q$ in Eq. [2] were equal to 1 and 2, respectively. We assume that the athermal stress $\tau_a$ is roughly equal to that measured by Conrad *et al.* in pure titanium of a similar grain size.[10] Finally, we restrict our investigation as much as possible to a regime where the deformation mechanisms remain uniform, utilizing TEM to verify this.

## III. EXPERIMENTAL

### A. *Material*

The material for this study was Ti-6-4 supplied in 13.8 mm thick plate. Results of a chemical analysis, determined by solution spectrographic analysis (for Ti, Al, V, and Fe) and mass spectroscopy (for O, N, and C), are as follows (in wt pct):

| Ti | Al | V | Fe | O | N | C |
|---|---|---|---|---|---|---|
| bal | 6.4 | 4.0 | 0.13 | 0.18 | 0.001 | 0.065 |

Compression tests were performed on material in the as-received (AR) starting condition, as well as in a solution treated (ST) and a solution treated and aged (AG) condition. Table I lists the heat treatment and describes the microstructure for each of these starting conditions. Note that TEM diffraction analysis showed intensity maxima at 0.5 [1010] positions. These could be due to short-range order (SRO) or very small $\alpha_2$ precipitates, either of which can form during slow cooling. (Both of these factors are known to enhance planar slip.) A TEM micrograph illustrating the fine, equiaxed grain structure in the hot worked and partially recrystallized AR condition is shown in Figure 1.

### B. *Compression Test Techniques*

Compression samples were tested as a function of temperature and strain rate and the data analyzed according to Eq. [2]. The deformation analysis described in Section II uses the mechanical threshold stress, or flow stress at 0 K, as an internal state variable, which is estimated by measuring the yield stress at low temperatures and extrapolating according to Eq. [2] to $T = 0$ K. For these measurements, a subpress submerged in a bath and attached to the crosshead of a standard screw-driven mechanical test machine was used. Liquid nitrogen was used at a temperature of 76 K,* while a liquid nitrogen/methanol bath was used for temperatures between 175 and 200 K. Displacement was measured with two LVDT's mounted off-axis between the platens and connected in

*Tests at temperatures less than 76 K, while possible, are not performed because of potential complications from viscous drag as 0 K is approached.

**Table I. Summary of Microstructural Conditions Investigated**

| Condition | Designation | Characterized Microstructure |
|---|---|---|
| As-received | AR | equiaxed $\alpha$ grain structure<br>grain size ≃ 5 $\mu$m<br>$\beta$ at grain boundary triple points<br>diffraction evidence of $Ti_3Al$ or SRO |
| As-received + solution treatment (800 °C, 1 h, water quench) | ST | same as in AR except: lower dislocation density, and no $Ti_3Al$ or SRO superlattice reflections |
| As-received + solution treatment + age (500 °C, 8 h) | AG | same as in ST except: strong $Ti_3Al$ or SRO superlattice reflections |

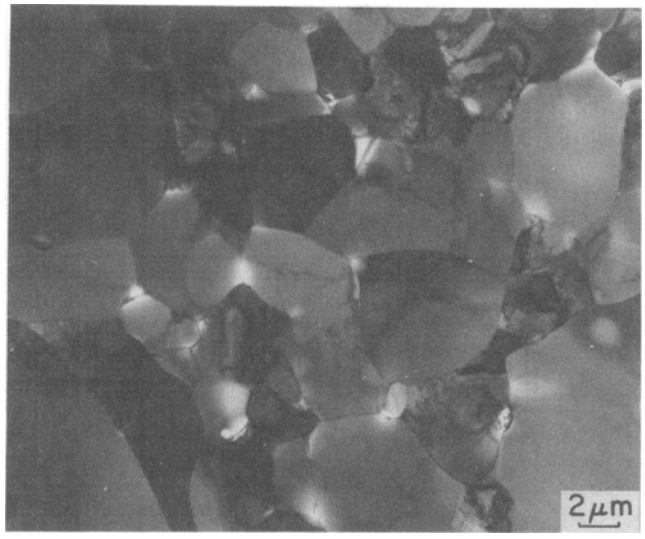


Fig. 1—TEM micrograph of the as-received (AR) Ti-6-4 microstructure.

series to cancel any bending motion. Lubrication at cold temperatures was achieved by coating the compression faces with a fine boron nitride commercial spray.

Some of the results presented below entail prestrains (duplicating each test condition with up to 10 specimens) according to a prescribed strain, strain rate, and temperature history, followed by a reload operation to determine the fit to Eq. [2]. Prestrains at room temperature and a strain rate of 0.001 $s^{-1}$ to strains of 0.101(∓0.002), 0.185(∓0.002), and 0.281(∓0.002) were performed in a standard screw-driven mechanical test machine. All specimens were machined such that, following the prestrain operations, the dimensions of the solid cylinders were roughly 4.8 mm diameter by 5.2 mm long. Prestrains at room temperature and a strain rate of 2500 $s^{-1}$ to a strain of 0.100(∓0.001) were performed in a split Hopkinson pressure bar (SHPB) using a 12.7 mm diameter transmitter bar with a 5.08 mm deep by 6.35 mm diameter flat-bottom hole at the specimen interface. Prestrains at 473 K and a strain rate of 0.001 $s^{-1}$ to a strain of 0.084(∓0.005) were performed in a vacuum furnace installed on a servohydraulic test machine.

Precise stress-strain measurements were not made during the prestrain operations because of mechanical constraints imposed to assure that each specimen was given the same strain. For the case of the SHPB specimens, for instance, more accurate measurements are obtained by using specimens with a length to diameter ratio of 0.6 and with a diameter less than the diameter of the pressure bar only by the desired amount of strain.[20] This precludes the use of the flat-bottom hole and introduces difficulties in precisely reproducing the final strain within each specimen. For the quasistatic strain rates, a donut insert was used around the specimen to assure uniform strain within each specimen. This procedure hindered the use of an extensometer close to the specimen at room temperature or the use of an optical diametrial extensometer at elevated temperature. Thus, stress-strain measurements for the prestrain conditions were made in separate tests configured for accurate strain measurements rather than for generating reproducible final strains.

### C. *Substructure Characterization*

Samples for optical metallography and TEM were sectioned from the as-received, heat treated, and deformed samples. TEM foils were prepared in a solution of 84 pct methanol, 10 pct butanol, and 6 pct perchloric acid at −40 °C with 10 volts using a Struer's Electropolisher. Observation of the foils was made using a JEOL 2000 EX at 200 kV equipped with a double-tilt stage.

## IV. RESULTS

### A. *Compression Test Results*

The strain-rate dependence of the yield stress and flow stress at $\varepsilon = 0.04$ on material in the AR starting condition is shown on semilogarithmic axes in Figure 2. Included with these data are measurements by several previous investigators on Ti-6-4 tested in tension,[21,22] as well as in compression[21,22,23] and at strain rates as high as 3000 $s^{-1}$.* In general, the results show a high strain-rate sensitivity of both the yield and flow stresses. The differences in flow stress levels between each set of data are believed to be related to differences in the microstructural conditions studied. Of these measurements, only those of Meyer[21] (in tension) suggest a strong increase in the strain-rate sensitivity at strain rates exceeding approximately $10^3$ $s^{-1}$, such as often observed in fcc metal.[24] However, tension test measurements by Harding on CP Ti[25] also indicated a trend toward an increased strain-rate sensitivity at strain rates exceeding $10^3$ $s^{-1}$.

*In comparing his measurements with previous measurements, Nicholas[22] includes a data point at $\dot{\varepsilon} = 1200$ $s^{-1}$ referenced to the work of Maiden and Green[23] but which is not found in Reference 23. We assume that this higher strain-rate datum was communicated later to Nicholas and also include it in our comparison in Figure 2.

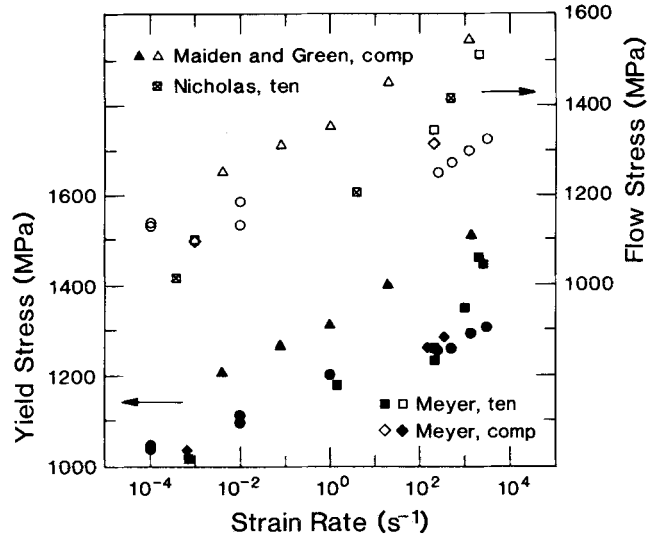


Fig. 2—Strain-rate dependence of the yield stress and flow stress at $\varepsilon = 0.04$ in Ti-6-4 and comparison with results of Meyer,[21] Nicholas,[22] and Maiden and Green.[23]

The variation of the reload yield stress with the reload test temperature ($\dot{\epsilon} = 0.001\ s^{-1}$) for the prestrain conditions noted is shown in Figure 3(a). All of the results shown in this figure were measured on material with the AR starting condition. The variation of yield stress *vs* test temperature for samples in the AR, ST, and AG conditions is shown in Figure 3(b).

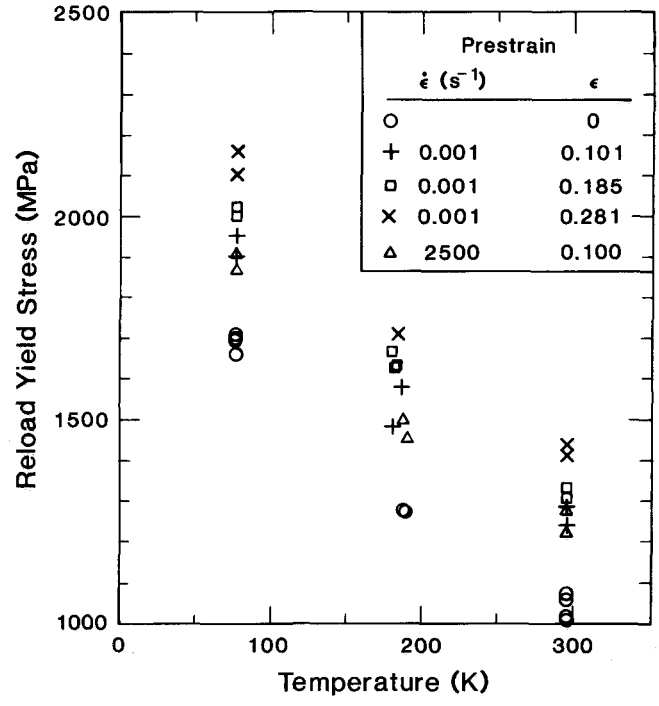


(*a*)

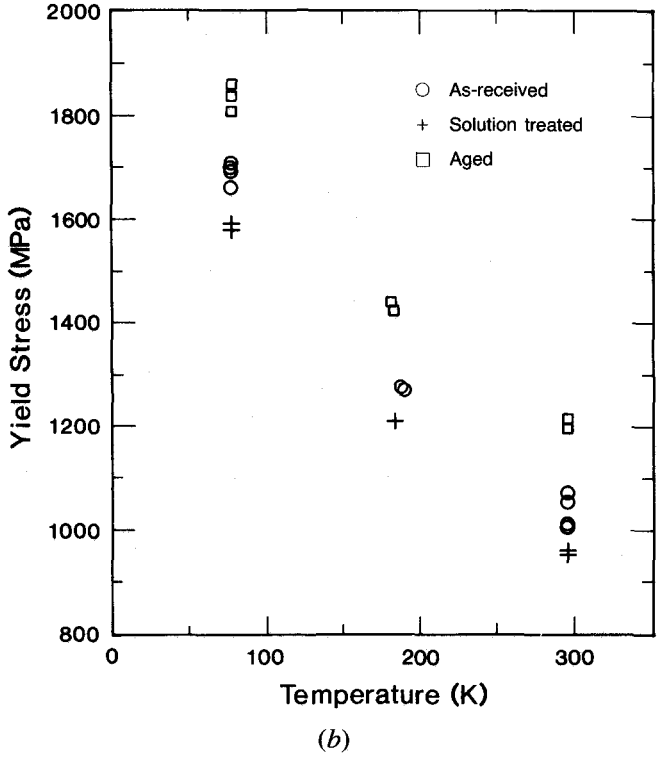


(*b*)

Fig. 3—Variation of the reload yield stress with reload test temperature for (*a*) material in the AR starting condition and prestrained according to the history specified; (*b*) material in the AR, ST, and AG starting conditions.

## B. *Substructure Characterization Following the Prestrains*

The substructure evolution of Ti-6-4 was found to depend on both the applied strain rate and the temperature of deformation. The equiaxed hcp alpha grains dominate the mechanical behavior of Ti-6-4 due to the high volume fraction of $\alpha$ in this alloy[26] and display the most evident changes in substructure with deformation history. The beta grains displayed no apparent change in substructure or morphology, and this observation was independent of deformation history. The substructure of Ti-6-4, deformed to a true strain of 0.101 at $\dot{\epsilon} = 0.001\ s^{-1}$, was characterized by planar slip bands within the alpha grains on prism, basal, and pyramidal planes (Figure 4). These planar dislocation arrays are similar to those known to dominate deformation behavior in Ti-Al alloys containing greater than 4 pct Al (by weight) and demonstrate that cross-slip is difficult in Ti-Al alloys at low temperature and high Al content.[5,27] The presence in the current Ti-6-4 alloy of SRO or fine $\alpha_2$ precipitates further favors concentration of dislocation activity into narrow slip bands.[27]

Samples strained an equivalent amount but at a strain rate of $5000\ s^{-1}$ displayed planar slip in the alpha grains, similar to those observed in the quasistatic samples, with the addition of numerous deformation twins, as seen in Figure 5. Twins were observed to have formed preferentially in grains whose mean size was larger than the average. The presence of twins corresponded to a decreased number of grains with planar slip as the sole deformation mechanism, suggesting a lower dislocation density which is consistent with the shear strain accommodation accompanying twins in titanium.[28]

Increasing the temperature of deformation to 200 °C

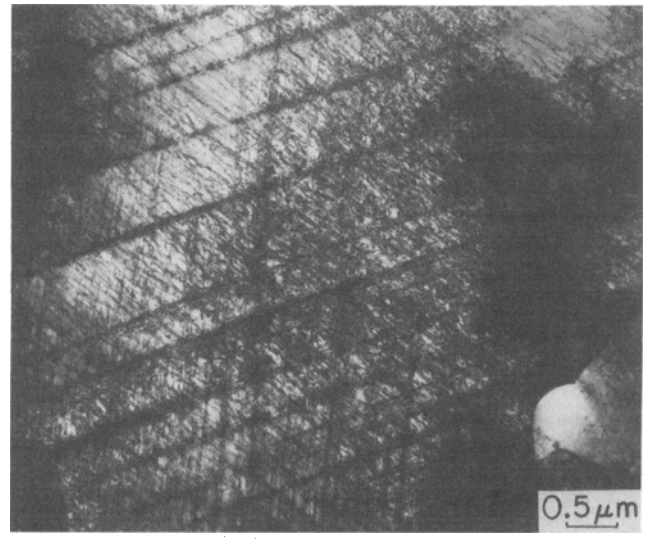


Fig. 4—TEM micrograph of Ti-6-4 deformed to a strain of $\varepsilon = 0.101$ at a strain rate of $\dot{\epsilon} = 0.001\ s^{-1}$, showing planar slip bands within the alpha grains.

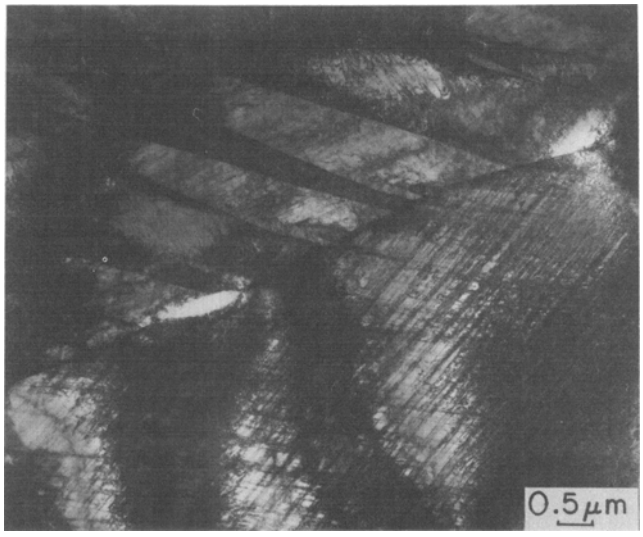


Fig. 5—TEM micrograph of Ti-6-4 deformed to a strain of $\varepsilon = 0.100$ at a strain rate of $\dot{\varepsilon} = 5000\ s^{-1}$, showing planar slip bands and deformation twins.

at $\dot{\varepsilon} = 0.001\ s^{-1}$ was seen to alter the dislocation morphology from solely that of planar slip bands to that of less coarse planar slip interspersed with random dislocation tangles (Figure 6). Increasingly random slip with increased temperature has been linked to the convergence of the resolved shear stress for prism, pyramidal, and basal slip in Ti-Al alloys at higher temperatures.[5] The tendency toward random dislocation arrangements indicates that, with increasing temperature, the stress for dislocation motion on the various slip planes becomes comparable, permitting easy cross slip which results in more random arrangements of dislocations.[5] Deformation twins were not observed in any samples deformed at 200 °C, which also follows from the ease of cross slip with increasing temperature.

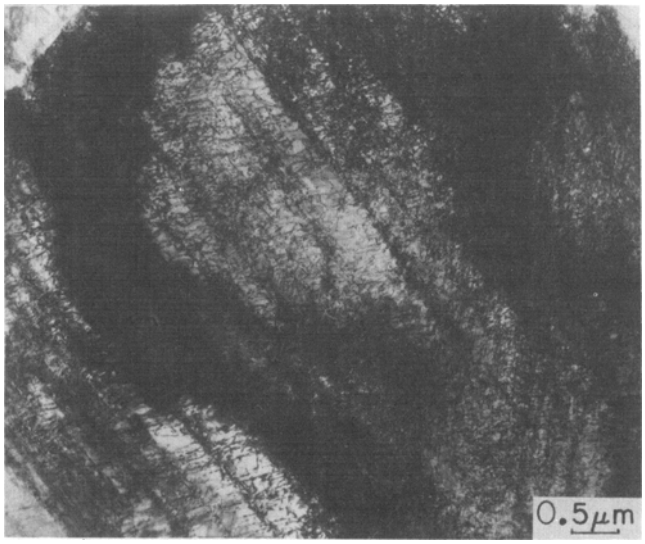


Fig. 6—TEM micrographs of Ti-6-4 deformed at 495 K to a strain of $\varepsilon = 0.084$ at a strain rate of $\dot{\varepsilon} = 0.001\ s^{-1}$, showing less coarse planar slip and random dislocation tangles.

## V. ANALYSIS AND DISCUSSION

### A. *Constant Structure*

Inspection of the results plotted in Figures 3(a) and (b) indicates that, over the temperature range tested, the yield stress is not a linear function of temperature. Analysis of these data reveals that Eq. [2] can be used to describe the curvature found in the yield stress *vs* temperature data if the individual contributions to the strengthening in Ti-6-4 can be represented. From the previous work on pure titanium,[8] dislocation/interstitial interactions are expected to be important. In Ti-6-4, we expect that the interaction of dislocations with solute atoms, primarily aluminum in $\alpha$ Ti grains, will also contribute to the thermal stress component. As previously indicated, dislocation/dislocation interactions will contribute to the strain-rate sensitivity of work hardened material. We assume that the athermal stress is due to long-range interactions (the most likely source being with grain boundaries, but perhaps also with the blocky $\beta$ phase). Accordingly, the athermal stress will be a small fraction of the yield stress, and its assumed value will have only a minor effect on the analysis of the results according to Eq. [2]. However, the inclusion of an athermal stress allows for the possibility of long-range interactions and illustrates how grain size effects or precipitates could be incorporated into the analysis outlined in Section II.

The variation of the shear modulus with temperature is modeled using the equation proposed by Varshni:[29]

$$\mu = \mu_o - \frac{a}{\exp(T_r/T) - 1}. \qquad [7]$$

To analyze the measurements on titanium-aluminum binary alloys by Paton *et al.*[5] (described in Section V–A–2), we use the data of Fisher and Renken[30] and take $\mu = (C_{44} \cdot C_{66})^{1/2} = [C_{44} \cdot (C_{11} - C_{12})/2]^{1/2}$, which can be fit to Eq. [7] with $\mu_o = 47.62$ GPa, $a = 5.821$, and $T_r = 181$ K. The temperature dependence of the shear modulus on the Ti-6-4 alloy studied in this work was measured[31] and fit to Eq. [7] with $\mu_o = 49.02$ GPa, $a = 4.355$, and $T_r = 198$ K.

#### 1. *The case of constant $\dot{\varepsilon}_o$, $p$, and $q$ values*

Although our goal is to separate the individual contributions to strengthening according to Eqs. [1] and [2], it is instructive to assume initially that $\dot{\varepsilon}_o$, $p$, and $q$ do not vary with obstacle type and to perform a least-squares fit of Eq. [2] to the data to determine the total mechanical threshold stress, $\hat{\sigma}$, and the net total activation free enthalpy, $g_o$. Figure 7 shows the fit of Eq. [2] to the yield stress measurements for material originally in the AR condition and prestrained at $\dot{\varepsilon} = 0.001\ s^{-1}$. The coordinates in Figure 7 have been chosen such that a straight line through the data points represents a fit according to Eq. [2] with $p = 1$ and $q = 2$. Included in the data for zero prestrain are reload yield stress measurements at strain rates of 250 to 3000 $s^{-1}$. An $\dot{\varepsilon}_o$ equal to $10^{10}\ s^{-1}$ gives the good agreement shown in Figure 7. Assuming that $\dot{\varepsilon}_o$, $p$, and $q$ remain constant with increasing strain, Figure 7 illustrates all of the data for prestrains for the AR condition, and Figure 8 shows the data for the three starting microstructural conditions. Table II summarizes the results from all of the microstructural and prestrain

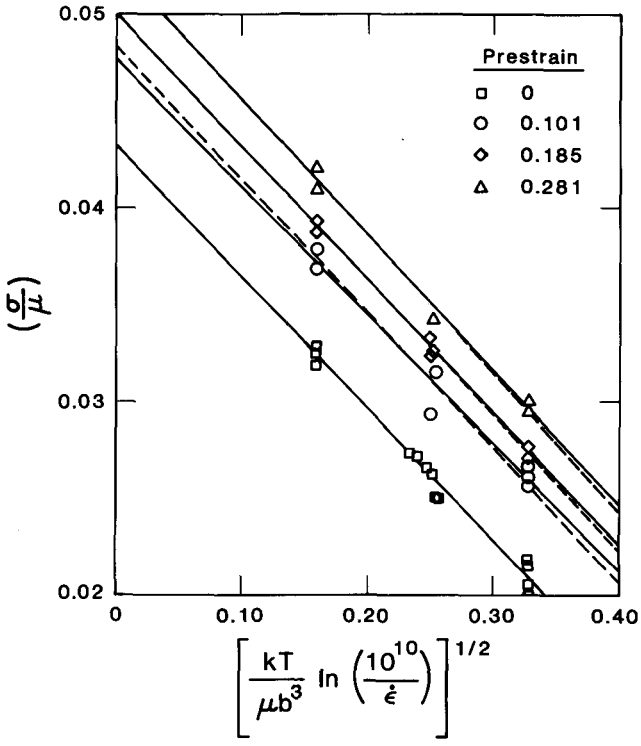


Fig. 7 — Variation of the reload yield stress with reload test temperature and strain rate for material in the AR starting condition. Solid line shows fit to Eq. [2], whereas dashed line shows fit to Eq. [11].

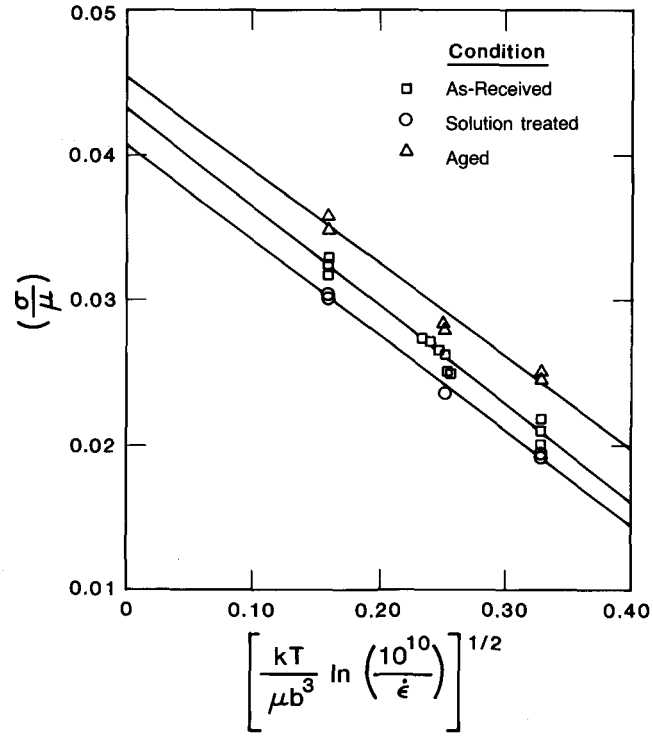


Fig. 8 — Variation of the reload yield stress with reload test temperature and strain rate for material in the AR, ST, and AG starting conditions. Results are fit to Eq. [2].

conditions.* Note in Table II that the mechanical threshold stress is seen to increase with increasing strain, reflecting the increasing dislocation density. Moreover, the normalized total activation free enthalpy, $g_o$, also increases with strain. This is due to the contribution of dislocation/dislocation interactions, which are relatively strong interactions characterized by longer range stress fields than are dislocation/interstitial or dislocation/solute atom interactions. Also note that the solution treatment results in a lower mechanical threshold stress and $g_o$ value than the as-received starting condition, due to the larger grain size, the more fully recrystallized structure produced, and the absence of $Ti_3Al$. Finally, aging the material increases the mechanical threshold stress as well as the normalized activation free enthalpy due to the contribution of the $Ti_3Al$ precipitates, which also are relatively long-range obstacles. The first-order assumption regarding the values of $\dot{\epsilon}_o$, $p$, and $q$ thus leads to variations in $\hat{\sigma}$ and $g_o$ that are consistent with our understanding of deformation mechanisms in this material.

*Equation [1] indicates that $\sigma_a/\mu$ and $\hat{\sigma}_i/\mu$ are constants. Thus, the values listed in Table II, and discussed below for convenience, are referenced to 295 K, where $\mu$ = 44.5 GPa.

2. *The case of variable $\dot{\epsilon}_o$, p, and q values*

Because the mechanical threshold stress is based upon an extrapolation according to a specific model, the values of $\hat{\sigma}$ listed in Table II depend on the assumptions made in formulating the model. In this section, we suggest a possible means to separate the influences of the various hardening mechanisms that influence the mechanical response of Ti-6-4. First, we estimate how the presence of solutes contributes to the interstitial hardening found in pure titanium. Paton *et al.* have measured the variation of yield stress with temperature in Ti-Al binary alloys as a function of aluminum content.[5] Figure 9 shows their results (in units of resolved shear stress) below a temperature of 373 K and the extrapolations to an aluminum content of zero that we have assumed. For these alloys, Eq. [1] reads (assuming linear summation):

$$\frac{\tau}{\mu} = \frac{\tau_a}{\mu} + s_I \frac{\hat{\tau}_I}{\mu} + s_S \frac{\hat{\tau}_S}{\mu} \qquad [8]$$

where

$$s_I = \left[1 - \left(\frac{kT}{g_{oI}\mu b^3} \ln \frac{\dot{\gamma}_{oI}}{\dot{\gamma}}\right)^{1/q_I}\right]^{1/p_I} \qquad [9]$$

and

$$s_S = \left[1 - \left(\frac{kT}{g_{oS}\mu b^3} \ln \frac{\dot{\gamma}_{oS}}{\dot{\gamma}}\right)^{1/q_S}\right]^{1/p_S} . \qquad [10]$$

Because the data of Paton *et al.*[5] are at a single strain rate and because data at temperatures greater than approximately 500 °C could reflect changing deformation mechanisms, we assume that the major difference between dislocation/interstitial and dislocation/solute interactions is the value of $g_o$, and we assume $p_I = p_S = 1$, $q_I = q_S = 2$, $\dot{\gamma}_{oI} = \dot{\gamma}_{oS} = 10^{10}\ s^{-1}$, and that $\tau_a$ (in units of resolved shear stress) equals 10 MPa. The fit of the data in Figure 9 to Eq. [8] is shown in Figure 10. For pure titanium a least-squares fit indicates that $g_{oI} = 0.264$ (in units of $\mu b^3$), which is consistent with the result of Conrad and coworkers.[6,8] A least-squares fit of Eqs. [8]

**Table II. Results of the Analysis According to Equation [2]**

| Starting Condition | Prestrain $\dot{\varepsilon}$ $s^{-1}$ | Prestrain $\varepsilon$ | Prestrain $T$ K | $\hat{\sigma}$ Mean MPa | $\hat{\sigma}$ S.E.* MPa | $g_o$ Mean ($\mu b^3$) | $g_o$ S.E.* ($\mu b^3$) |
|---|---|---|---|---|---|---|---|
| AR | — | none | — | 2023 | 24 | 0.41 | 0.04 |
| AR | 0.001 | 0.101 | 295 | 2218 | 53 | 0.52 | 0.11 |
| AR | 0.001 | 0.185 | 295 | 2322 | 17 | 0.53 | 0.03 |
| AR | 0.001 | 0.281 | 295 | 2435 | 35 | 0.57 | 0.07 |
| AR | 2500 | 0.100 | 295 | 2186 | 39 | 0.51 | 0.08 |
| AR | 0.001 | 0.084 | 495 | 2039 | 41 | 0.57 | 0.11 |
| ST | — | none | — | 1909 | 18 | 0.38 | 0.03 |
| AG | — | none | — | 2117 | 41 | 0.50 | 0.09 |

*Standard error of estimate.

through [10] to the data in Figure 9 can be used to establish $g_{os}$ and $\hat{\tau}_S$ values for each aluminum content. However, an essential feature of our analysis is that a single value of $g_{os}$, along with a $\hat{\tau}_S$ value that depends on aluminum content, should closely fit the data. Indeed, a value of $g_{os} = 0.8$ gives a good overall fit to the data, as shown in Figure 10. The resulting $\hat{\tau}_S$ values are included in Figure 10. It is evident that the concentration dependence is stronger than the square-root relationship given in Eq. [4]. Paton *et al.*[5] noted that the tendency toward deformation twinning decreased with increasing aluminum content, which could explain the higher yield stress for the highest aluminum content. Similarly, Paton *et al.*[5] found that the extent of slip planarity varied with aluminum content. These findings emphasize that the complex deformation mechanisms in titanium alloys may have subtle effects that are difficult to fully describe quantitatively. Nonetheless, the simple analysis outlined by Eqs. [8] through [10] provides insight into the key features of these deformation mechanisms. The results indicate that the contribution of solution strengthening adds a less strain-rate sensitive obstacle to the interstitial effect present in the pure material.

To add the contribution of dislocation/dislocation interactions for the strain-hardened material and to reflect the uniaxial stress state in a compression test, we rewrite Eq. [1] as

$$\frac{\sigma}{\mu} = \frac{\sigma_a}{\mu} + s_I \frac{\hat{\sigma}_I}{\mu} + s_S \frac{\hat{\sigma}_S}{\mu} + s_D \frac{\hat{\sigma}_D}{\mu} \qquad [11]$$

where

$$s_D = \left[1 - \left(\frac{kT}{g_{o_D}\mu b^3} \ln \frac{\dot{\varepsilon}_{o_D}}{\dot{\varepsilon}}\right)^{1/q_D}\right]^{1/p_D} . \qquad [12]$$

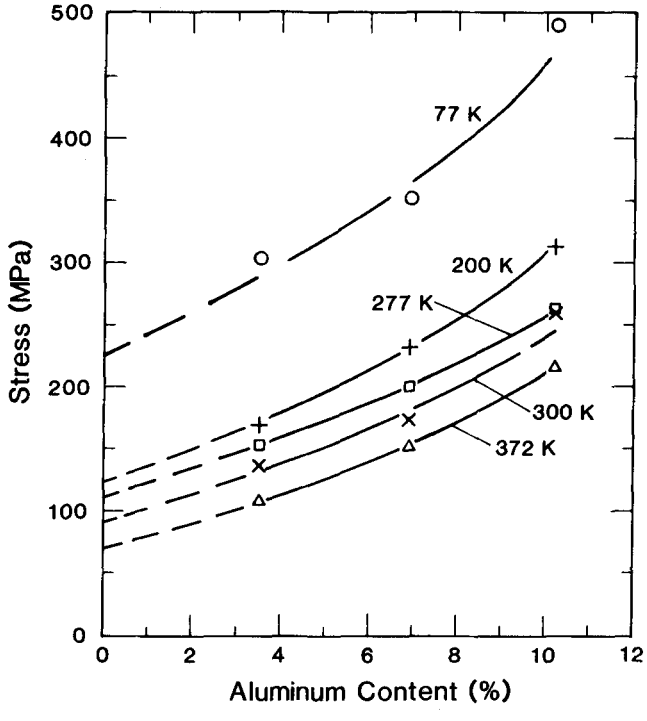


Fig. 9—Results of Paton *et al.* in Ti-Al binary alloys,[5] showing the variation of yield stress (in shear) with temperature as a function of aluminum atomic percent.

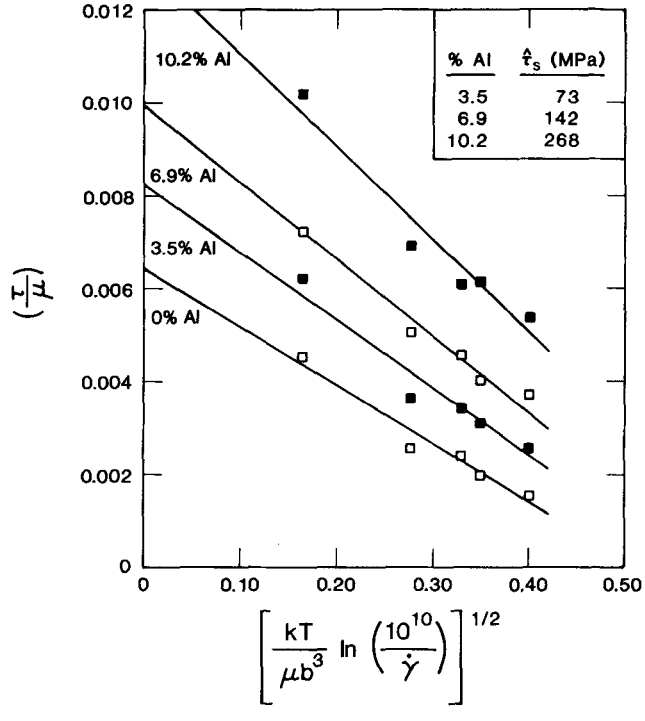


Fig. 10—Results of Paton *et al.*[5] replotted using normalized yield stress and temperature and strain-rate coordinates and fit according to Eq. [8]. For pure titanium, the mechanical threshold stress ($\hat{\tau}_I$) equals 262 MPa.

We assume that dislocation/interstitial interactions are represented by $g_{o_I} = 0.264$; the dislocation/solute interactions are represented by $g_{o_S} = 0.8$; and that the values of $q_I$, $q_S$, $p_I$, $p_S$, $\dot{\gamma}_{o_I}$, and $\dot{\gamma}_{o_S}$ are as established in the previous paragraph. (In equating $\dot{\gamma}_o$ to $\dot{\varepsilon}_o$ we are ignoring a Taylor factor, but this is not significant when compared to the experimental uncertainty in this pre-exponential factor.) For the athermal stress in Ti-6-4, we choose $\sigma_q = 100$ MPa. This value is higher than that assumed for analysis of the Paton *et al.* results because of the difference in stress units (resolved shear stress *vs* uniaxial normal stress) and because the grain size in the Ti-6-4 material is considerably smaller than that in the Ti-Al binary (5 $\mu$m *vs* 30 $\mu$m). First, we establish $\hat{\sigma}_I$ and $\hat{\sigma}_S$ by fitting Eq. [11] to the data in the AR condition, where the dislocation density is found to be low, and, thus, we can assume that $\hat{\sigma}_D = 0$. The resulting fit yields $\hat{\sigma}_I = 1050$ MPa and $\hat{\sigma}_S = 873$ MPa.

With $\hat{\sigma}_I$ and $\hat{\sigma}_S$ established (along with $g_{o_I}$ and $g_{o_S}$), we can proceed to the cases where $\hat{\sigma}_D \neq 0$. Again, there are insufficient data over a wide strain rate and temperature regime to allow an independent evaluation of $g_{o_D}$, $\dot{\varepsilon}_{o_D}$, $q_D$, and $p_D$. Following previous work,[14] therefore, we choose $g_{o_D} = 1.6$ to characterize the strong, long-range interactions between dislocations and choose $q_D = 1$ and $p_D = 2/3$ to reflect the different, statistically averaged shape of the obstacle profile.[14] For consistency with the previous results in copper,[14] the pre-exponential factor $\dot{\varepsilon}_{o_D}$ is chosen as $10^7$ s$^{-1}$, although because $\dot{\varepsilon}_{o_D}$ is found within a logarithmic term in Eq. [12], variations in $\dot{\varepsilon}_{o_D}$ of several orders of magnitude have only a minor influence on the predictions. The remaining unknown in Eq. [11] is $\hat{\sigma}_D$ which can be determined from a fit of the data to Eq. [11]. The results for measurements on material in the AR condition are summarized in Table III. Comparison of the results (particularly for the variation of $\hat{\sigma}$ with strain) in Tables II and III indicates that, while the estimated $\hat{\sigma}$ values do vary with the assumptions of the model, they are not overly sensitive to these assumptions (*i.e.*, the estimated $\hat{\sigma}$ values listed in Tables II and III agree within 2 pct). The fits to the data for prestrains at $\dot{\varepsilon} = 0.001$ s$^{-1}$ are shown as dashed lines in Figure 7. Note that these fits essentially are indistinguishable from the fits according to Eq. [2] also shown in this figure.

Results for the dynamic prestrains, also included in Table III, indicate that the estimated mechanical threshold stress is less than that for quasistatic prestrain to the same strain. It was noted above that deformation twinning was observed in the dynamically deformed samples but not in the quasistatically deformed material. The threshold stress measurements are consistent with this observation, which suggests that during dynamic deformation some of the imposed strain has been accommodated by twinning, leading to a lower dislocation density and mechanical threshold stress. The implication here is that deformation twins in Ti-6-4 do not act as obstacles to dislocation motion and, thereby, influence the mechanical threshold stress.

For the samples deformed at 495 K, we note that the agreement between the results of the two approaches summarized in Tables II and III is not very good, and that the standard errors for the estimates of $\hat{\sigma}$ shown in Tables II and III are larger than for the other estimates listed in these tables. Although these disparities may reflect the difficulty in obtaining precise prestrain deformation at elevated temperature, the lower threshold stress listed in Table II may also indicate a dynamic recovery contribution of the partially recrystallized starting material or be due to the presence of SRO or $\alpha_2$, which have not been encountered during deformation at the higher temperature and, thus, provide a long-range (less strain-rate sensitive) obstacle to dislocation motion.

### 3. *High strain-rate deformation*

The results discussed above at constant structure imply that deformation at strain rates well within (and even above) those achieved in the SHPB will remain in the thermally activated controlled regime. It has been shown that a transition from thermally activated controlled deformation to dislocation drag controlled deformation requires stresses on the order of or greater than the mechanical threshold stress.[32,33] Because the measured yield stresses in Ti-6-4, even at strain rates to 3000 s$^{-1}$, are below the estimated mechanical threshold stresses, we conclude that the deformation mechanism at these high strain rates remains thermal activation and that the yield stress *vs* strain-rate relation should follow the mild strain-rate dependence of Eq. [2] at strain rates up to and even exceeding those reached in the Hopkinson bar. Yield stress measurements that show a dramatically increasing strain-rate sensitivity at high strain rates, such as reported by Meyer[21] and Harding,[25] are inconsistent with this interpretation. It is interesting that the yield stress measurements reported by both of these investigators were made in dynamic tension tests.

**Table III. Results of the Analysis According to Equation [11]**

| Prestrain | | | | $\hat{\sigma}$ | |
|---|---|---|---|---|---|
| $\dot{\varepsilon}$, s$^{-1}$ | $\varepsilon$ | $T$, K | $\hat{\sigma}_D$, MPa | Mean, MPa | S.E.,* MPa |
| — | none | — | 0 | 2023 | 24 |
| 0.001 | 0.101 | 295 | 229 | 2252 | 56 |
| 0.001 | 0.185 | 295 | 309 | 2332 | 19 |
| 0.001 | 0.281 | 295 | 413 | 2436 | 36 |
| 2500 | 0.100 | 295 | 195 | 2218 | 42 |
| 0.001 | 0.084 | 495 | 121 | 2144 | 67 |

*Standard error of estimate.

Although tension tests at high strain rates are particularly difficult to perform and interpret,[34] the tension test usually produces more uniform loading rates at yield than achieved in compression using Hopkinson bar techniques; it is possible that in a well-annealed sample with a low initial dislocation density, high stress levels would be required at yield to generate and move the dislocations at the rates necessary to accommodate the imposed deformation. This, in fact, is the mechanism thought to be responsible for the rapid strain hardening in copper and other fcc metals at high strain rates.[14,35] If dynamic tension tests do lead to more rapid dislocation generation than found in dynamic compression tests, then one would expect recovered tensile specimens to be harder than compression specimens deformed to the same strain.

### B. *Structure Evolution*

The variation of $\hat{\sigma}_D$ with strain for quasistatic prestrains is shown in Figure 11 along with the fit of the Voce law (Eq. [5] with $F = 1$). The equation for the solid line through the data points is written as

$$\hat{\sigma}_D = \hat{\sigma}_{Ds}\left[1 - \exp\left(\frac{-\Theta_o \varepsilon}{\hat{\sigma}_{Ds}}\right)\right] \qquad [13]$$

where $\hat{\sigma}_{Ds} = 538$ MPa and the athermal hardening rate, $\Theta_o$ (in uniaxial stress-strain units), is found to equal 2721 MPa (or $\mu/16.3$). Equation [6] implies that the saturation stress should be strain-rate and temperature dependent, but clearly there are insufficient data in the measurements reported here to establish these dependencies. If the strain-rate and temperature dependencies arise from a dynamic recover (*via* cross-slip) mechanism, then the strain-rate dependence of $\hat{\sigma}_{Ds}$ is positive which is in the opposite direction to the trend found, albeit at a single strain. As noted above, however, deformation twinning was observed in the dynamically deformed samples. The reload data suggest that the occurrence of deformation twinning leads to a lower rate of dislocation generation (evolution) than would be expected for dislocation activity alone.

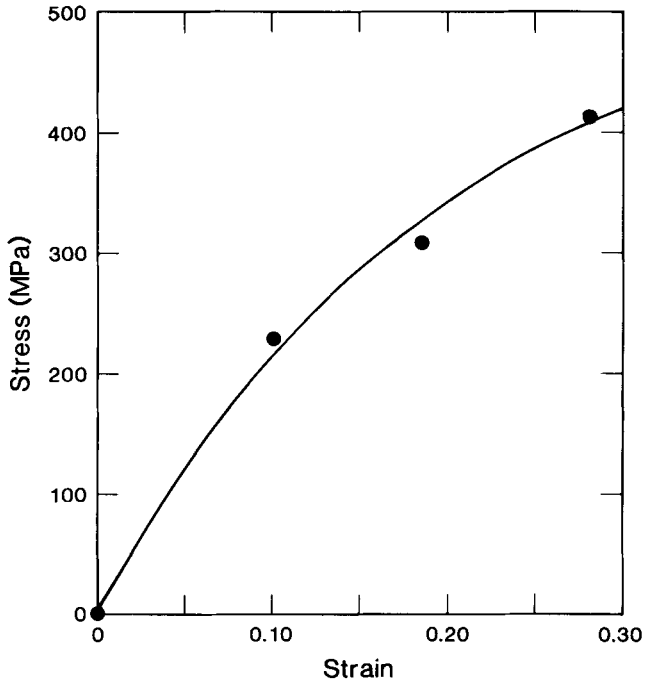


Fig. 11—Variation of the mechanical threshold stress characterizing dislocation/dislocation interactions ($\hat{\sigma}_D$) with strain and fit of the results to the Voce law (Eq. [5] with $F = 1$).

The temperature dependence of $\hat{\sigma}_D$ (at 10 pct strain) is negative which is consistent with Eq. [6]. However, we suspect that the measured decrease in $\hat{\sigma}_D$ for the 495 K prestrain is larger than it would be if the predominance for coarse planar slip had not changed at the higher temperature.

### C. *Application of the Model*

Although there are more parameters in the approach outlined in Section V–A–2 (Eqs. [9] through [12]) than in the approach outlined in Section V–A–1, the latter is preferred to the former, because it results in a single strain-dependent variable ($\hat{\sigma}_D$), whereas the latter results in two strain-dependent variables ($\hat{\sigma}$ and $g_o$). Therefore, Eqs. [9] through [12] will be used for the constant structure component of our model. For the structure evolution component, we apply Eq. [13] and assume (by necessity) that the saturation stress is strain-rate and temperature independent. This simplifies the solution of the equations to calculate stress-strain behavior, because it implies that Eq. [13] can be used for any strain rate and temperature history to predict the evolution of $\hat{\sigma}_D$. The applied stress for a specified temperature and strain rate then is computed using Eq. [9] and Eqs. [10] through [12] for $s_I$, $s_S$, and $s_D$.

An example of the prediction of the model is shown in Figure 12, which shows the computed stress-strain behavior (solid line) and measured data for a prestrain at 189 K and a strain rate of 0.0015 $s^{-1}$ to a plastic strain of 0.131, followed by unloading and reloading at 295 K and a strain rate of 0.001 $s^{-1}$. There is a slight indication that the strain hardening rate at the lower temperature is higher than predicted, which is consistent with the expected temperature dependence of $\hat{\sigma}_{Ds}$.

A second example of the application of the model is shown in Figure 13, which shows the experimental data and model prediction for a strain rate of 3000 $s^{-1}$ and an initial temperature ($T_o$) of 295 K. Note that there are two curves shown—one for isothermal conditions ($T$ = 295 K) and one for adiabatic conditions ($T_o$ = 295 K). For the latter prediction, it is assumed that 90 pct of the plastic work is converted to heat; the temperature rise is calculated by dividing this energy by $\rho \cdot c_p$ (2.33 MPa/K). It is expected that a strain rate of 3000 $s^{-1}$ is well into the adiabatic regime. Indeed, the curve calculated assuming adiabatic conditions is considerably closer to the experimental results than is the corresponding curve for isothermal conditions. The pronounced effect shown in Figure 13 arises from the high strength of Ti-6-4, coupled with the high temperature dependence of the flow stress, which makes this alloy particularly susceptible to shear localization during adiabatic deformation.[36,37,38] A final example showing a prestrain at $\dot{\varepsilon} = 2500$ $s^{-1}$ to a strain of $\varepsilon = 0.10$ (adiabatic deformation at $T_o$ =

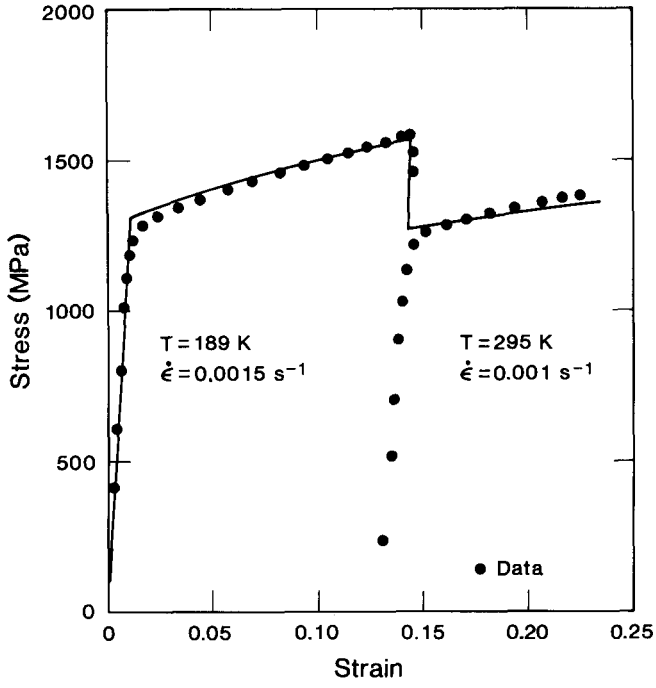


Fig. 12—Model prediction and comparison with experimental results for a prestrain at $T$ = 189 K and $\dot{\epsilon}$ = 0.0015 s$^{-1}$ to $\epsilon$ = 0.131, followed by unloading and reloading at $T$ = 295 K and $\dot{\epsilon}$ = 0.001 s$^{-1}$.

295 K) followed by unloading and reloading at $\dot{\epsilon}$ = 0.0015 s$^{-1}$ (isothermal deformation at $T$ = 295 K) is shown in Figure 14. As in Figure 13, the measured dynamic flow stresses are slightly less than predicted, which we believe is related to the contribution of deformation twinning.

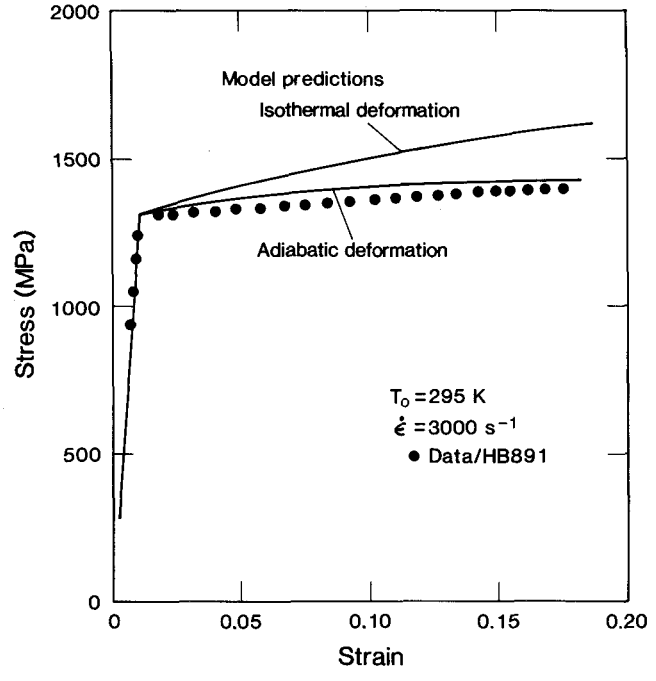


Fig. 13—Model prediction and comparison with experimental results for deformation at $T_o$ = 295 K and $\dot{\epsilon}$ = 3000 s$^{-1}$. Predictions for adiabatic and isothermal deformation are shown.

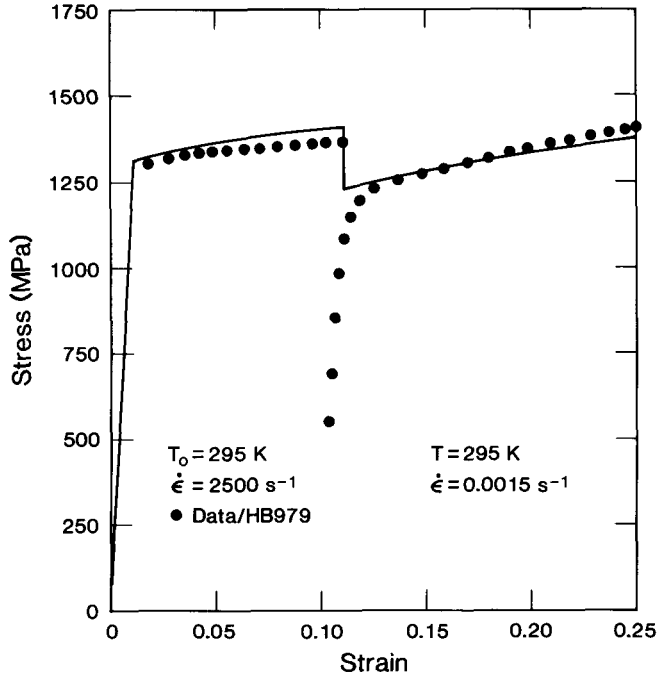


Fig. 14—Model prediction and comparison with experimental results for a prestrain at $T_o$ = 295 K and $\dot{\epsilon}$ = 2500 s$^{-1}$ to a strain of $\epsilon$ = 0.10 (assumed to be adiabatic), followed by unloading and reloading at $T$ = 295 K and $\dot{\epsilon}$ = 0.0015 s$^{-1}$.

## VI. SUMMARY

The examples shown in Figures 12 through 14 demonstrate that constitutive equations based on the Kocks/Mecking model can predict both monotonic deformation behavior, as well as the response to path changes involving dramatic or gradual variations in temperature and strain rate. We have emphasized that the analysis which we have applied to the deformation of Ti-6-4 is valid over a relatively narrow regime of conditions. Changes in slip character or in deformation mechanism (*e.g.*, deformation twinning) have been observed to correlate with changes in the expected behavior and have led to results that cannot be described with the procedures outlined in this paper without the addition of more state variables or at least allowing variations in the parameters characterizing dislocation/obstacle interactions.

The contribution made in the work presented here is the successful application in a relatively complex alloy system of a model of deformation based on an understanding of the kinetics of dislocation/obstacle interactions and of structure evolution. An apparent disadvantage of the analysis described in Section V is the number of fitting parameters in Eqs. [9] through [12]. Values of these parameters, however, are constrained within well-defined limits. Our approach has not been to search for values of these parameters that yield the closest agreement with experimental results and to allow variations of these parameters with strain, for instance, but rather to verify that Eqs. [9] through [12] with constant (and theoretically plausible) values of $g_{oI}$, $g_{oS}$, $g_{oD}$, $\dot{\epsilon}_{oI}$, *etc.*, can be used to model deformation in Ti-6-4. The preferred form of the model is that described in Section V–A–2, because it includes only the state parameters $\hat{\sigma}_I$, $\hat{\sigma}_S$, and

$\hat{\sigma}_D(\varepsilon)$ and the constants in Eqs. [9] through [12] that characterize in a statistical sense the individual dislocation/obstacle interactions. The benefit of such an analysis is that it leads to a physically motivated set of equations and, thus, a deeper correlation between constitutive equations and operative deformation mechanisms.

## ACKNOWLEDGMENTS

The authors are grateful for the technical assistance of M.F. Lopez and W.J. Wright in performing the tests described herein. We also are grateful for technical discussions regarding this work with J.C. Williams, and the advice and suggestions for further work that grew out of this collaboration. This work was supported by the United States Department of Energy, Office of Basic Energy Sciences, Division of Materials Sciences.

## REFERENCES

1. C. Hammond and J. Nutting: *Metal Science*, 1977, vol. 11, pp. 474-90.
2. E.W. Collings: *The Physical Metallurgy of Titanium Alloys*, ASM, Metals Park, OH, 1984.
3. U.F. Kocks: *J. Eng. Mater. and Tech.*, 1976, vol. 98, pp. 76-85.
4. H. Mecking and U.F. Kocks: *Acta Metall.*, 1981, vol. 29, pp. 1865-75.
5. N.E. Paton, J.C. Williams, and G.P. Rauscher: *Titanium Science and Technology*, R.I. Jaffee and H.M. Burte, eds., Plenum Press, New York, NY, 1973, pp. 1049-69.
6. H. Conrad: *Acta Metall.*, 1966, vol. 14, pp. 1631-33.
7. B. de Meester, M. Döner, and H. Conrad: *Zeitschrift für Metallkunde*, 1973, vol. 64, pp. 775-81.
8. H. Conrad, M. Döner, and B. de Meester: *Titanium Science and Technology*, 2nd Int. Conf., R.I. Jaffee and H.M. Burte, eds., Plenum Press, New York, NY, 1973, pp. 969-1005.
9. R.R. Zeyfang and H. Conrad: *Zeitschrift für Metallkunde*, 1975, vol. 66, pp. 422-27.
10. K. Okazaki and H. Conrad: *Japan Institute of Metals*, Transactions, 1972, vol. 13, pp. 205-13.
11. U.F. Kocks, A.S. Argon, and M.F. Ashby: *Progress of Materials Science*, Pergamon Press, New York, NY, 1975, vol. 19, pp. 139-43.
12. U.F. Kocks: *Strength of Metals and Alloys*, ICSMA 5, P. Haasen, V. Gerold, and G. Kostorz, eds., Pergamon Press, Toronto, 1980, pp. 1661-80.
13. P. Haasen: *Phil. Mag.*, 1958, vol. 3, pp. 384-418.
14. P.S. Follansbee and U.F. Kocks: *Acta Metall.*, 1988, vol. 36, pp. 81-93.
15. R.N. Orava, G. Stone, and H. Conrad: *Trans. ASM*, 1966, vol. 59, pp. 171-84.
16. B. de Meester, M. Döner, and H. Conrad: *Metall. Trans. A*, 1975, vol. 6A, pp. 65-75.
17. P.P. Tung and A.W. Sommer: *Metall. Trans.*, 1970, vol. 1, pp. 947-53.
18. J.I. Dickson, L. Handfield, and G. L'Espérance: *Metall. Trans. A*, 1985, vol. 16A, pp. 694-95.
19. A.M. Garde, A.T. Santhanam, and R.E. Reed-Hill: *Acta Metall.*, 1972, vol. 20, pp. 215-20.
20. C.E. Frantz, P.S. Follansbee, and W.J. Wright: *High Energy Rate Fabrication*, I. Berman and J.W. Schroeder, eds., ASME, New York, NY, 1984, pp. 229-36.
21. L.W. Meyer: *Titanium, Science and Technology*, G. Lütjering, U. Zwicker, and W. Bunk, eds., Deutsche Gesellschaft für Metallkunde, 1984, pp. 1851-58.
22. T. Nicholas: *Experimental Mechanics*, 1981, vol. 38, pp. 177-85.
23. C.J. Maiden and S.J. Green: *J. Appl. Mech.*, 1966, vol. 33, pp. 496-504.
24. P.S. Follansbee: *Metallurgical Applications of Shock-Wave and High-Strain-Rate Phenomena*, L.E. Murr, K.P. Staudhammer, and M.A. Meyers, eds., Marcel Dekker, New York, NY, 1986, pp. 451-79.
25. J. Harding: *Archives of Mechanics*, 1975, vol. 27, pp. 715-32.
26. M. Peters and G. Luetjering: *Titanium' 80*, Proc. of the 4th Int. Conf. on Titanium, H. Kimura and O. Izumi, eds., TMS-AIME, Warrendale, PA, 1980, pp. 925-35.
27. M.J. Blackburn and J.C. Williams: *Trans. AIME*, 1969, vol. 62, pp. 398-409.
28. N.E. Paton and W.A. Backofen: *Metall. Trans.*, 1970, vol. 1, pp. 2839-47.
29. Y.P. Varshni: *Physical Review B*, 1970, vol. 2, no. 10, pp. 3952-58.
30. E.S. Fisher and C.J. Renken: *Physical Review*, 1964, vol. 135, no. 2A, pp. A482-A494.
31. P.E. Armstrong: Los Alamos National Laboratory, Los Alamos, NM, unpublished research, 1986.
32. P.S. Follansbee, G. Regazzoni, and U.F. Kocks: *Mechanical Properties at High Rates of Strain*, J. Harding, ed., Institute of Physics, London, 1984, Ser. 70, pp. 71-80.
33. G. Regazzoni, U.F. Kocks, and P.S. Follansbee: *Acta Metall.*, 1987, vol. 35, pp. 2865-75.
34. G. Regazzoni, J.N. Johnson, and P.S. Follansbee: *J. Appl. Mech.*, 1986, vol. 108, pp. 519-28.
35. P.S. Follansbee: *Impact Loading and Dynamic Behaviour of Materials*, C. Y. Chiem, H.-D. Kunze, and L. W. Meyer, eds., Informationsgesellschaft, 1988, pp. 315-22.
36. R.F. Recht: *J. Appl. Mech.*, 1964, vol. 31E, pp. 189-93.
37. R. Dormeval and M. Stelly: *High Energy Rate Fabrication*, 7th Int. Conf., University of Leeds, 1981, pp. 1-9.
38. S.P. Timothy and I.M. Hutchings: *Acta Metall.*, 1985, vol. 33, pp. 667-76.